

Proceedings of the
III Int. School and Symposium on Physics in Materials Science, Jaszowiec '98

MUON SPIN ROTATION STUDIES OF DOPING IN HIGH- T_c SUPERCONDUCTORS

CH. NIEDERMAYER

Fakultät für Physik, Universität Konstanz, 78457 Konstanz, Germany

Muon spin rotation studies on high temperature superconducting cuprates will be reviewed. After an introduction to the technique, studies on the superfluid density will be described and the universal variation of the superfluid density n_s as a function of p will be presented. Important exceptions will be discussed, such as the $\text{YBa}_2\text{Cu}_3\text{O}_{7-\delta}$ system, where, besides the intrinsically superconducting CuO_2 planes, an interlayer may be metallised (here the CuO chains) which consequently contributes to a significant enhancement in superfluid density and associated improvement in technologically interesting properties such as flux pinning and critical current density. Evidence for an unconventional pairing state, possibly with d -wave symmetry, is presented from studies of the rapid suppression of superfluid density due to the substitution of structural inhomogeneities (such as Zn) that introduce strong scattering centers within the CuO_2 planes. Finally, the phase diagram of the antiferromagnetic correlations and, in particular, their coexistence with the superconducting state, will be discussed in terms of muon spin rotation experiments in zero external magnetic field.

PACS numbers: 74.25.Ha, 74.62.Dh, 76.75.+i

1. Introduction

The technique of muon spin rotation or relaxation (μSR) is a powerful tool for studying the internal distribution of magnetic fields within solids [1]. In the context of high temperature superconducting (HTS) cuprates μSR experiments have provided important contributions to a better understanding of the physics of the vortex state, superfluid density and the complex interplay between magnetism and superconductivity that distinguishes the HTS cuprates. These materials are strongly anisotropic due to their distinctive structure which comprises quasi-two-dimensional CuO_2 planes separated by insulating interlayers. The electronic correlations causing magnetism and superconductivity originate primarily in the CuO_2 planes. One of the most striking features of the HTS cuprates is the strong dependence of these electronic correlations on the hole concentration per CuO_2 plane, p , resulting in a generic p -dependent phase behavior as summarised in

Fig. 1. At very low doping these materials are antiferromagnetic (AF) insulators but with increasing p the AF correlations are weakened and the Néel temperature, T_N , falls rather sharply to zero. At a critical concentration there occurs an insulator–metal transition coinciding with the onset of superconductivity. The critical temperature $T_c(p)$ follows a universal, approximately parabolic p -dependence that can be conveniently expressed as [2]

$$T_c = T_{c,\max} [1 - 82.6(p - 0.16)^2], \quad (1)$$

where the maximum is reached for an optimum doping of $p \approx 0.16$ holes per CuO_2 plane. This p -dependence appears to be common to the HTS cuprates and all that varies between the different HTS compounds is the magnitude of the optimal value, $T_{c,\max}$. As also shown in the figure, at intermediate doping levels extending from the Néel state and well into the superconducting domain, short-ranged AF fluctuations survive and at low temperatures freeze into a disordered spin-glass state (annotated SG) which co-exists with superconductivity.

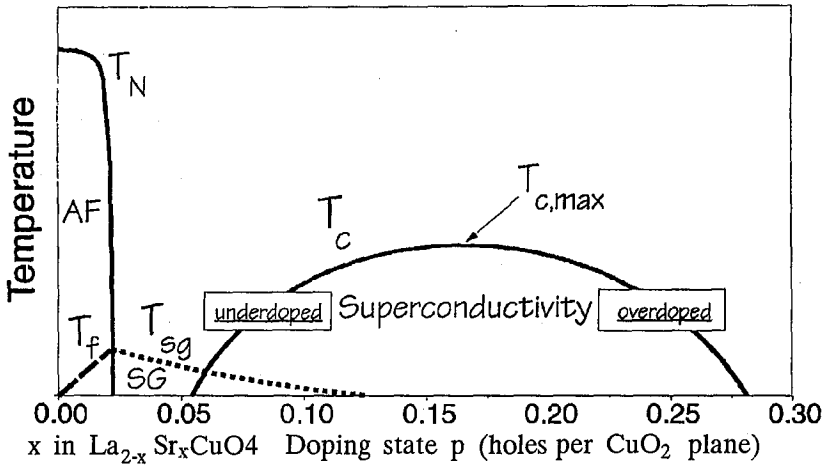


Fig. 1. Schematic representation of the doping-dependent phase diagram for HTS cuprates. AF and SG denote the antiferromagnetic and spin-glass phases.

After an introduction to the technique, studies on the superfluid density will be described and the universal variation of the superfluid density n_s as a function of p will be presented. Important exceptions will be discussed, such as the $\text{YBa}_2\text{Cu}_3\text{O}_{7-\delta}$ system, where, besides the intrinsically superconducting CuO_2 planes, an interlayer may be metallised (here the CuO chains) which consequently contributes to a significant enhancement in superfluid density and associated improvement in technologically interesting properties such as flux pinning and critical current density. Evidence for an unconventional pairing state, possibly with d -wave symmetry, is presented from studies of the rapid suppression of superfluid density due to the substitution of structural inhomogeneities (such as Zn) that introduce strong scattering centers within the CuO_2 planes. Then, μSR studies revealing new and exotic transitions in the vortex state of highly anisotropic cuprate systems (such as $\text{Bi}_2\text{Sr}_2\text{CaCu}_2\text{O}_8$) will be discussed. Finally, the phase diagram of the

antiferromagnetic correlations and, in particular, their coexistence with the superconducting state, will be discussed in terms of μ SR experiments in zero external magnetic field.

2. The μ SR technique

The basic idea of a μ SR experiment is very similar to that of the NMR technique. Positive muons are incorporated as local probes in the host lattice of the sample to be studied. The spin of the muon and the related magnetic moment act as a sensitive probe for the local magnetic field through its precession in the field with a frequency of $\omega_\mu = \gamma_\mu B_{\text{loc}}$, where $\gamma_\mu = 851.4$ MHz/T is the gyromagnetic ratio of the muon and B_{loc} is the local field. The polarisation of the muon is conveniently determined by the fact that when a muon decays (half life $2.2 \mu\text{s}$) the resulting positron is emitted preferentially in the direction of the instantaneous polarisation. A schematic diagram of the standard μ SR experiment is shown in Fig. 2. A beam of 100% spin-polarised muons is directed onto the cuprate sample which, for studies of the vortex state and superfluid density, is mounted in a magnetic field of strength H transverse to the polarisation of the muon spin. The sample may be a sintered polycrystalline body, an oriented single crystal, a mosaic of single crystals or even a compact of powder. The injected muons thermalise rapidly without any significant loss in polarisation and come to rest at locations in the sample which are random on a scale of the London penetration depth, λ (100–300 nm) but at distinct sites in the crystallographic unit cell, forming a muoxyl bond with apical or chain oxygens [3]. The muon spin precesses about the local field which may be modulated due to flux vortices in the presence of the field but may, in zero field, arise from magnetic ordering or local moments. In the transverse-field experiment, the precession frequency is randomly distributed due to the random distribution of local fields and so the muons dephase and progressively lose their polarisation. The time-resolved polarisation signal is thus oscillatory with decaying amplitude. Its depolarisation rate provides a measure for the inhomogeneity of the magnetic field in the vortex state and hence for the magnetic penetration depth. By Fourier transformation one can obtain the frequency-resolved signal which in the case of single-crystalline materials exhibits the characteristic features of the vortex structure, i.e a tail towards high frequencies (fields) caused by the vortex cores, a peak at the field of the saddle point between two vortices and a sharp cut-off on the low field side. For polycrystalline samples the distribution of precession frequencies is almost symmetrical and of approximately Gaussian shape. In this case, the Gaussian depolarisation rate, σ , may be found from the second moment $\langle \Delta\omega^2 \rangle$ of the frequency distribution or more conveniently it may be more directly determined from the envelope of the oscillatory time-resolved polarisation, as given by

$$P(t) \propto \exp(-\sigma^2 t^2 / 2). \quad (2)$$

The key factor is that σ , being a measure of the field distribution, is proportional to $\lambda_{\text{eff}}^{-2}$, where λ_{eff} is an effective magnetic penetration depth related to the in-plane and out-of-plane penetration depths λ_{ab} and λ_c by the degree of anisotropy and field orientation. As such it is a measure of the superfluid density, n_s , as will be seen.

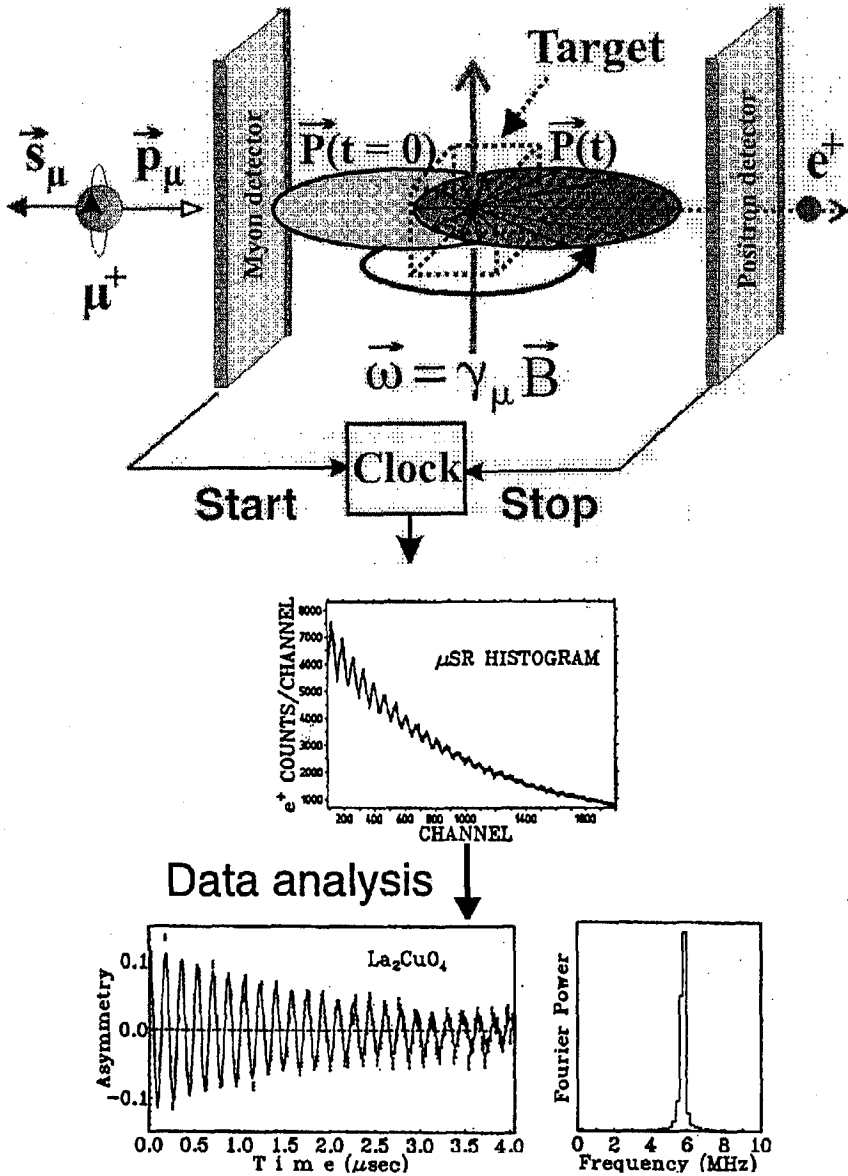


Fig. 2. Schematic diagram showing the main components of the μ SR technique.

Barford and Gunn [4] have analysed the situation for highly anisotropic systems such as the HTS cuprates and find for a polycrystalline sample that $\lambda_{\text{eff}} = 1.23 \times \lambda_{ab}$ provided that the anisotropy $\lambda = \lambda_c / \lambda_{ab} > 5$, which is generally satisfied. They deduce

$$\sigma [\mu\text{s}^{-1}] = 7.086 \times 10^4 \times \lambda_{ab}^{-2} [\text{nm}] \quad (3)$$

$$= 2.75 \times 10^9 n_s / m_{ab}^* [\text{cm}^{-3} \text{kg}^{-1}]. \quad (4)$$

Here n_s is the superfluid density expressed as the density of *single* quasiparticles which contribute to the condensate, and m_{ab}^* is the electronic effective mass for a - b plane transport. We stress that for an ideal homogeneous superconductor in the absence of pairbreaking the low-temperature superfluid density is expected to be equal to the carrier concentration.

3. Superconducting condensate density

The early μ SR studies on the cuprates appeared largely confined to underdoped and near optimally doped samples. This led to the remarkable observation by Uemura and coworkers [5, 6] that, for a wide range of cuprates, T_c and the low temperature depolarisation rate are linearly related

$$T_c \propto \sigma_0 \propto \lambda_0^{-2} \propto n_s(T=0)/m^*, \quad (5)$$

where λ and m are to be understood as λ_{ab} and m_{ab} . This relationship is shown in Fig. 3. This universal linearity was taken at the time to be evidence of the superconducting transition being a Bose-Einstein condensation of performed real-space pairs [5] in which

$$T_c \propto E_F = \pi \hbar^2 n/m^* \quad (6)$$

for a 2D free-electron gas. While this view continues to maintain some support it is not upheld by heat capacity measurements. Dissociation of pairs at elevated

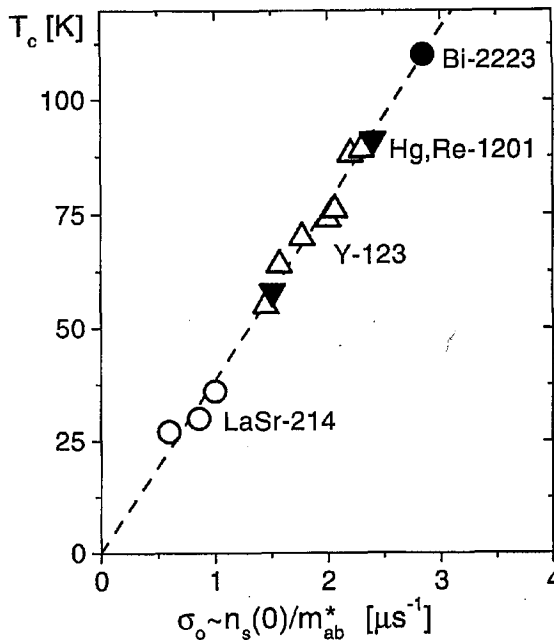


Fig. 3. T_c plotted as a function of the μ SR depolarisation rate for underdoped cuprates showing the universal linear relation $T_c \sim \sigma_0 \sim n_s/m^*$.

temperatures would lead to a clear increase in entropy/ T which is not evident [7]. Several alternative models have been shown to lead to this key $T_c \propto \sigma_0$ relationship (see [8] and references therein).

For quite some time the expectation was that the superfluid density $n_s(T=0)$ should continue to increase with growing carrier concentration in the overdoped regime. Experimentally it was found that n_s was strongly depressed in the overdoped region so that T_c versus $n_s(T=0)$ follows a reentrant loop as shown in Fig. 4. This behavior was first demonstrated for the $\text{Tl}_2\text{Ba}_2\text{CuO}_{6+\delta}$ system [9–11] and later reproduced for $\text{Yb}_{0.7}\text{Ca}_{0.3}\text{Ba}_{1.6}\text{Sr}_{0.4}\text{Cu}_3\text{O}_{7-\delta}$ [12], a system, in which the hole concentration can be varied throughout the entire range from heavily underdoped to heavily overdoped. This behavior was modelled in terms of intrinsic pairbreaking progressively developing on the overdoped side [9, 10] and providing an increasing density of normal-state carriers. This view was underscored by heat capacity measurements on the same samples of Tl-2201 [13] which showed the low-temperature linear coefficient of the electronic heat capacity, γ_0 , progressively rising with overdoping from zero towards the normal-state value, γ_n , well above T_c . This increasing density of low-energy excitations is strongly sugges-

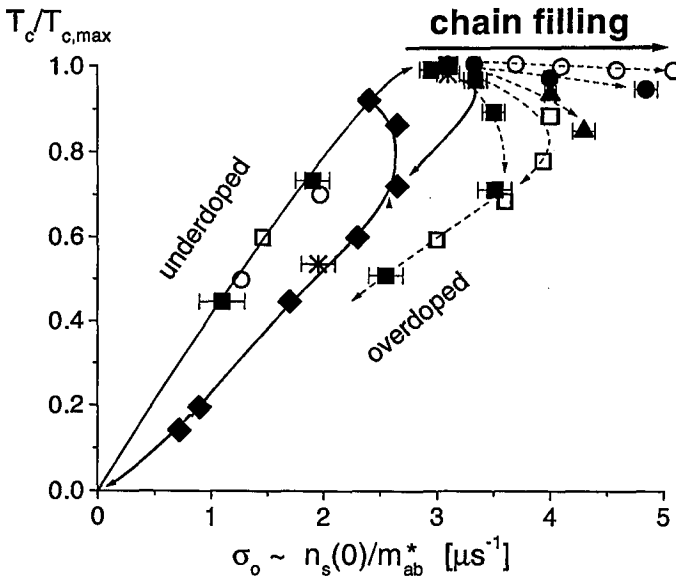


Fig. 4. $T_c/T_{c,max}$ plotted as a function of the μSR depolarisation rate extending from the under- to overdoped region showing the generic re-entrant loop behavior on the overdoped side. The “plane+chain” samples of $\text{Y}_{1-x}\text{Ca}_x\text{Ba}_2\text{Cu}_3\text{O}_{7-\delta}$ are represented by (o) for $x = 0$, (●) $x = 0.03$, (full triangle) $x = 0.13$, (□) $x = 0.2$ and (■) for $\text{Yb}_{0.7}\text{Ca}_{0.3}\text{Ba}_{1.6}\text{Sr}_{0.4}\text{Cu}_3\text{O}_{7-\delta}$. The broad plateau occurs for $\delta < 0.15$. Here σ_0 doubles as the chains become fully oxygenated. “Plane-only” samples are (full diamond) $\text{Tl}_2\text{Ba}_2\text{CuO}_{6+\delta}$, (*) $\text{Y}_{1-x}\text{Ca}_x\text{Ba}_2\text{Cu}_3\text{O}_{6.2}\text{Br}_x$ ($x = 0$ and $x = 0.2$) and the highly deoxygenated “plane+chain” samples ($\delta > 0.3$).

tive of pair breaking. The suppressed condensate density was confirmed in Tl-1212, La-214 and in Ca-substituted $\text{R}\text{Ba}_2\text{Cu}_3\text{O}_{7-\delta}$ with $\text{R} = \text{Y}$ and Yb [14] and may be considered to be a generic effect amongst the cuprates. More recent infrared reflectivity measurements on overdoped Bi-2212 confirm the reduction in λ_{ab}^{-2} and at the same time show a dramatic filling of the gap in $\sigma(\omega)$ with overdoping and an increase in elastic scattering [15].

In contrast, $\text{YBa}_2\text{Cu}_3\text{O}_{7-\delta}$ develops a broad plateau as $\delta \rightarrow 0$ (open circles in Fig. 4). An important structural aspect of this high T_c -superconductor is the presence of linear CuO-chains in addition to the CuO_2 -planes. We have argued that upon full oxygenation the chains become metallic and n_s rapidly increases due to the additional condensate density induced there [14, 16]. To further elucidate this chain condensation we studied a series of $\text{Y}_{1-x}\text{Ca}_x\text{Ba}_2\text{Cu}_3\text{O}_{7-\delta}$ with $x = 0.03, 0.06, 0.13, 0.2$ and $\text{Yb}_{0.7}\text{Ca}_{0.3}\text{Ba}_{1.6}\text{Sr}_{0.4}\text{Cu}_3\text{O}_{7-\delta}$. In this 1-2-3 system hole doping of the CuO_2 -planes is not only achieved by oxygenation of the CuO-chains but also by replacing Y^{3+} by Ca^{2+} . With increasing Ca-content the complete oxygenation of the CuO-chains is thus shifted towards the overdoped regime. While for $x = 0$ the final filling of the CuO-chains coincides with optimum doping in the planes ($T_{c,\text{max}}$) and one therefore observes the well known "plateau" in σ_0 versus T_c , the "plateau" disappears gradually with increasing Ca-content and is completely

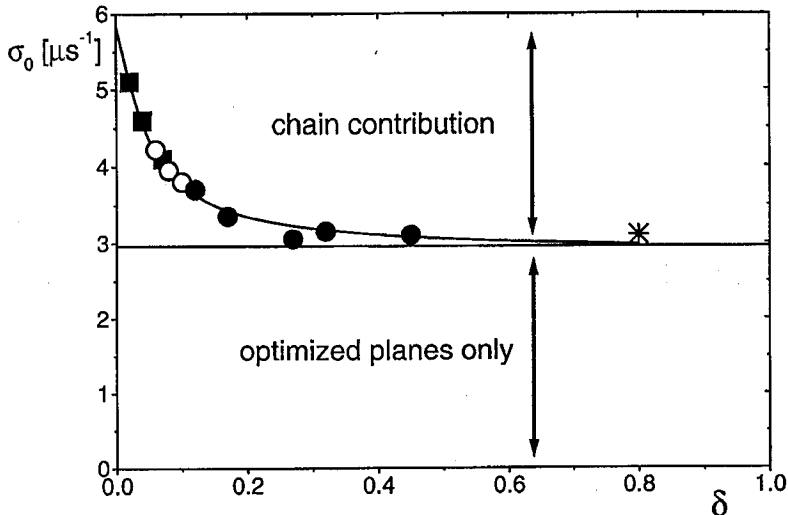


Fig. 5. The low temperature depolarisation rate σ_0 for optimally doped $\text{Y}_{1-x}\text{Ca}_x\text{Ba}_2\text{Cu}_3\text{O}_{7-\delta}$ as a function of the oxygen deficiency, δ ; (o) $\text{TmBa}_2\text{Cu}_3\text{O}_{7-\delta}$; (■) slightly overdoped $\text{YBa}_2\text{Cu}_3\text{O}_{7-\delta}$ for $\delta = 0.02, 0.04,$ and 0.07 ; (●) optimised samples for $x = 0, 0.03, 0.06, 0.13,$ and 0.20 and (*) $\text{YBa}_2\text{Cu}_3\text{O}_{6.2}\text{Br}_z$ with $T_c = 92$ K. The solid line is a fit by a model, where the chain condensate is mobile just along the CuO-chains and suppressed by pairbreaking effects that are caused by randomly distributed oxygen vacancies.

absent for $x = 0.2$ and 0.3 . In these compounds the planes are already overdoped when the additional chain-condensate is formed.

To separate the chain and plane contributions to the superconducting condensate density, we performed μ SR-experiments on samples with optimally doped CuO_2 -planes but with different degrees of chain filling. The results for σ_0 versus oxygen deficiency δ are shown in Fig. 5. For all samples with $\delta > 0.3$ we observe the same value of $\sigma_0 \sim 3.0(1) \mu\text{s}^{-1}$, which therefore represents the contribution of the CuO_2 -planes to the condensate density. The additional contribution due to the appearance of superconductivity in the chains is only observed for samples with lower oxygen deficiencies ($\delta < 0.25$). The solid line is a fit by a model where the additional chain condensate is mobile just along the CuO -chains and rapidly destroyed by pair-breaking due to oxygen vacancies, which we assume to be randomly distributed. We deduce a chain-coherence length of $\xi_0^{\text{ch}} = 5.6 \text{ nm}$ and a pronounced in-plane anisotropy with $\lambda_a = 150 \text{ nm}$ and λ_b as low as 80 nm . Such an in-plane anisotropy for λ_b and λ_a is confirmed by microwave experiments [17].

Cu nuclear quadrupol resonance experiments provide information on the average length n of the ordered chain-fragments [18]. For (Y,Gd,Tm)-123 Lütgemeier et al. observe a sharp increase in n when $\delta < 0.25$, most probably because the oxygen vacancies tend to form clusters. Comparing their data with our μ SR-results (open circles in Fig. 5) we find that the increase in n is correlated to the growth of the chain-condensate. Rather short chain-fragments (due to a random distribution of the O-vacancies) are found in the case of $\text{NdBa}_2\text{Cu}_3\text{O}_{7-\delta}$. Consequently, the observed σ_0 -value of $2.85 \mu\text{s}^{-1}$ for $\text{NdBa}_2\text{Cu}_3\text{O}_{6.94}$ nearly equals that of a slightly underdoped “plane-only” sample. These results indicate that the chain-condensate is extremely sensitive on any disruption of the long range order in the CuO -chains.

4. Symmetry of the superconducting order parameter

The substitution of Zn for Cu has attracted much attention because it suppresses T_c exceptionally fast while not altering the carrier concentration of the CuO_2 sheets. While the rapid depression of T_c may be explained by magnetic pair breaking for any symmetry of the order parameter, the variation of n_s upon impurity concentration is predicted to depend very sensitively on the symmetry of the order parameter [19]. In Fig. 6 we plot the ratio of the condensate density measured in $\text{Y}_{0.8}\text{Ca}_{0.2}\text{Ba}_2(\text{Cu}_{1-y}\text{Zn}_y)_3\text{O}_{7-\delta}$ and $\text{La}_{1.79}\text{Sr}_{0.21}\text{Cu}_{1-y}\text{Zn}_y\text{O}_4$ relative to that obtained for the Zn-free sample as a function of the relative depression of the critical temperature. A satisfactory description of the very rapid initial decrease (for low Zn content) in the condensate density requires a model based on a $d_{x^2-y^2}$ -wave order parameter (OP) (or another unconventional OP which changes a sign in k -space) in which Zn causes a strong potential scattering in the unitarity limit as shown by the solid line. The corresponding behavior for an s -wave OP (where T_c is substantially reduced only by magnetic scattering) is shown for the so called “clean limit” ($\ell \gg \xi_0$, dotted line) and the “dirty limit” ($\ell \gg \xi_0$, dash-dot line [20]), where ξ_0 is the superconducting coherence length and ℓ is the transport mean free path. For more details see Ref. [21].

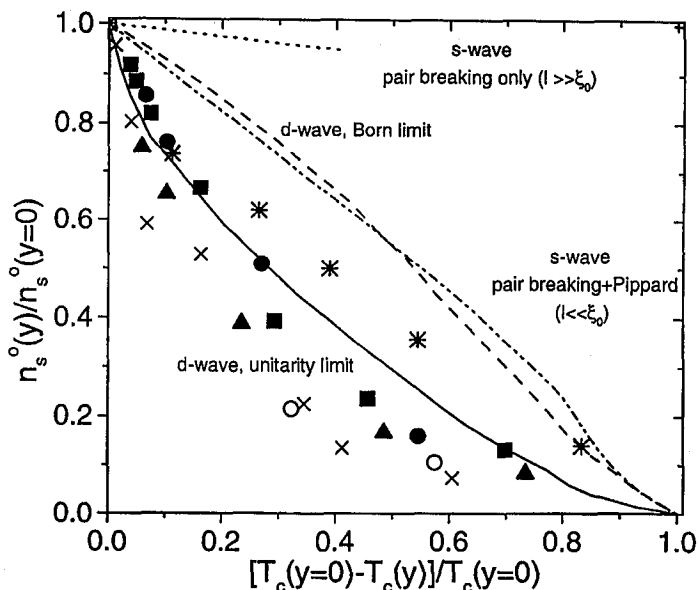


Fig. 6. The depression of the normalised superconducting condensate density $n_s^0(y)/n_s^0(y=0)$ plotted as a function of the relative decrease in T_c . Data are shown for the under- (\bullet), optimally- (\blacksquare) and overdoped series (full triangle) of $Y_{0.8}Ca_{0.2}Ba_2(Cu_{1-y}Zn_y)_3O_{7-\delta}$ and for overdoped $La_{1.79}Sr_{0.21}Cu_{1-y}Zn_yO_4$ (\circ). The crosses represent some of our previous results for almost fully oxygenated $YBa_2(Cu_{1-y}Zn_y)_3O_{7-\delta}$. Asterisks show the data for optimally doped to overdoped $Tl_2Ba_2CuO_{6+\delta}$. The expected behavior for a $d_{x^2-y^2}$ symmetry of the OP and non-magnetic elastic scattering in the unitarity limit (Born limit) is shown by the solid (dashed) line. The corresponding case of an isotropic s -wave OP with magnetic scattering is shown by the dotted (dashed dotted) line for the “clean” (“dirty”) limit.

5. Antiferromagnetism and superconductivity in HTS cuprates

Whenever the insulating composition of a given class is chemically stable, it generally exhibits a long-range AF order that is rapidly destroyed by small amounts of doped carriers. Short-range 2D AF correlations, however, persist into the superconducting regime. It is therefore of great importance to study the evolution of magnetism as more holes are doped into the CuO_2 -planes and to explore the interplay between the short-range magnetic order and superconductivity.

The zero-field (ZF) μ SR technique is especially suited for such studies since the positive muon is an extremely sensitive local probe able to detect internal magnetic fields as small as 0.1 mT and covering a time window from 10^{-6} s to about 10^{-10} s. Another advantage is the sensitivity of the muon probe to extremely short-ranged magnetic correlations. Systematic studies so far focused on the La-214 [22, 23] and Y-123 [24, 25] systems. In Y-123 the phase diagram has to be drawn versus oxygen content and a reliable determination of p is difficult due to the rather complicated charge transfer from the CuO -chains to the CuO_2 -planes. The $Y_{1-x}Ca_xBa_2Cu_3O_6$ system, i.e. with $\sigma = 1.0$, avoids this complication, because hole doping is achieved by the substitution of Y^{3+} by Ca^{2+} . This allows

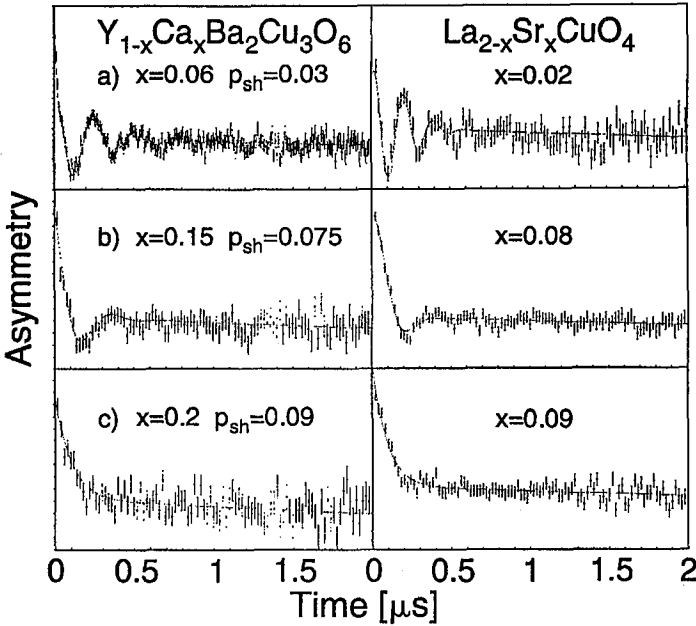


Fig. 7. ZF- μ SR spectra obtained at low temperatures ($T < 1$ K) for various degrees of hole doping in $Y_{1-x}Ca_xBa_2Cu_3O_{6.02(1)}$ and $La_{2-x}Sr_xCuO_4$. Dotted curves are the fit to the data using Eq. (7).

one to directly control the hole concentration in the CuO_2 -planes in a quantitative manner and $p = x/2$.

Representative ZF- μ SR time spectra are shown in Fig. 7. At low temperature and for $p \leq 0.08$, the time evolution of the muon spin polarization is well described by the ansatz

$$G_z(t) = \frac{2}{3} \cos(\gamma_\mu B_\mu t + \Phi) \exp\left[-\frac{1}{2}(\gamma_\mu \Delta B_\mu t)^2\right] + \frac{1}{3} \exp(-\lambda t), \quad (7)$$

where $\gamma_\mu = 851.4$ MHz/T is the gyromagnetic ratio of the muon, B_μ the average internal magnetic field at the muon site and ΔB its rms deviation. The two terms arise from the random orientation of the local magnetic field in a polycrystalline sample, which on average points parallel (perpendicular) to the muon spin direction with probability 1/3 (2/3) [1]. In analogy to NMR the dynamic spin lattice relaxation rate $\lambda = 1/T_1$ is given by

$$\frac{1}{T_1} = \gamma_\mu^2 \langle B_t^2 \rangle \frac{\tau_c}{1 + (\omega_\mu \tau_c)^2}. \quad (8)$$

A slowing down of magnetic fluctuations typically causes a maximum of $1/T_1$ at $\omega_\mu \tau_c \approx 1$, where ω_μ is the μ^+ Zeeman frequency, $\langle B_t^2 \rangle$ — the mean of the square of the fluctuating transverse field components and τ_c their average correlation time. A precessing 2/3 component indicates static magnetic order on the time scale of the μ SR technique ($\tau_c < 10^{-6}$ s). For $p > 0.08$ no oscillations were observed and the 2/3 part of $G_z(t)$ was better represented by an exponential relaxation $\exp(-\lambda t)$ (see Fig. 7c), which may indicate either a very strongly disordered static field distribution or rapid fluctuations.

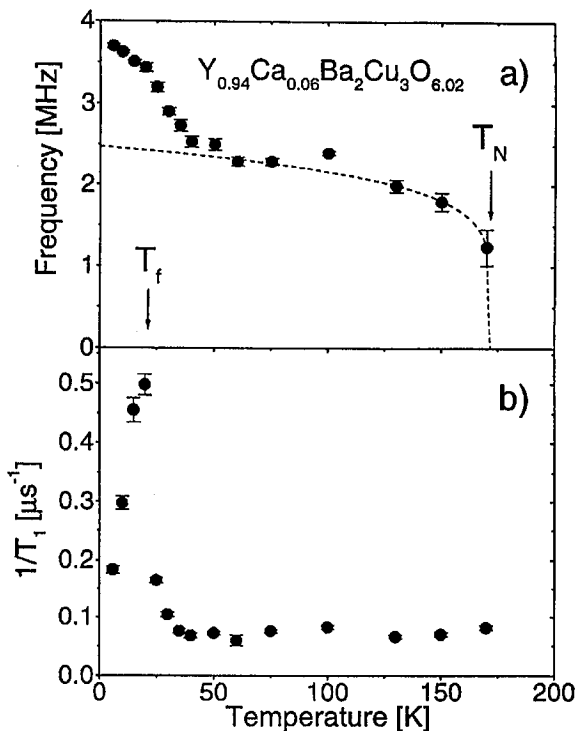


Fig. 8. ZF- μ SR results on $\text{Y}_{0.94}\text{Ca}_{0.06}\text{Ba}_2\text{Cu}_3\text{O}_{6.02(1)}$ plotted as a function of temperature. (a) The muon spin precession frequency and (b) the longitudinal relaxation rate $1/T_1$. The dotted line in (a) represents a fit of the data with a power law $(1 - T/T_N)^\beta$ with $\beta = 0.2$.

For only lightly doped systems the Cu^{2+} spins and those of the holes order independently. As an example we discuss the data on $\text{Y}_{0.94}\text{Ca}_{0.06}\text{Ba}_2\text{Cu}_3\text{O}_{6.02}$ which are displayed in Fig. 8. Well below the 3D Néel temperature of $T_N \approx 170$ K a second magnetic transition occurs at a temperature $T_f \approx 25$ K. This is evident from the peak in the longitudinal relaxation rate $1/T_1$ and the upturn of the muon spin precession frequency. A corresponding transition within the AF state has been reported recently from La-NQR [26] and μ SR studies [27] on La,Sr-214, where $T_f = (815 \text{ K})p$ has been obtained for $p < 0.02$. This transition was ascribed to a freezing of the spins of the doped holes into a spin-glass state which is superimposed on the preexisting 3D AF long-range order of the Cu^{2+} spins. Interestingly, we find that the spin freezing temperature T_f exhibits the same linear dependence on the planar hole content for Y,Ca-123 and La,Sr-214 (see Fig. 9). According to the model of Gooding et al. [28], in which $k_B T_f \approx J_{\text{eff}} p$, this implies that the effective in-plane exchange coupling constant, J_{eff} , is identical for both systems and that the freezing of the spin degrees of freedom is a property of the hole dynamics within a single plane. The Néel-state, however, persists to a higher hole content in Y,Ca-123 ($0 \leq p \leq 0.035$) as compared to La,Sr-214 ($p \leq 0.02$). This suggests that the bilayer coupling makes the 3D AF-state more robust to the presence of doped holes. A similar result was reported from a ^{89}Y NMR study of T_N in Y,Ca-123 [29].

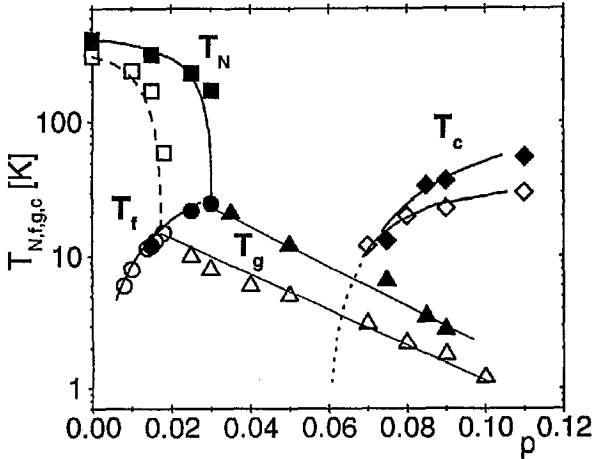


Fig. 9. Magnetic phase diagram as a function of the hole concentration per CuO_2 sheet for $\text{La}_{2-x}\text{Sr}_x\text{CuO}_4$ (open symbols) and $\text{Y}_{1-x}\text{Ca}_x\text{Ba}_2\text{Cu}_3\text{O}_{6.02}$ (full symbols). For only lightly doped systems two transitions are observed. The Néel temperatures T_N (squares), at which the Cu^{2+} spins order into a 3D AF state and a freezing transition of the spins of the doped holes at $T_f = (815 \text{ K})p$ (circles, including the data from Ref. [27]). T_g (triangles) indicates a transition into a spin-glass-like state with strong magnetic correlations which coexist with superconductivity for $p > 0.06$. Diamonds represent the superconducting transition temperatures.

Only a single magnetic transition into a short-range AF correlated spin-glass-like state is observed for $p > 0.02$ in La,Sr-214 and $p > 0.035$ in Y,Ca-123. This transition is characterized by a slowing down of the AF fluctuations towards a glass transition which is defined by the maximum in $1/T_1$ (corresponding to a correlation time of the spin fluctuations of about 10^{-7} s). The spin-glass character of this magnetic state has been demonstrated recently for $\text{La}_{1.96}\text{Sr}_{0.04}\text{CuO}_4$, where the susceptibility exhibits irreversible and remanent behavior and obeys scaling laws [30]. T_g is significantly higher due to bilayer interactions in Y,Ca-123 than in La,Sr-214.

It is notable that spin-glass behavior is observed for both compounds up to about $p = 0.11$, the same point where static susceptibility, spin susceptibility and heat capacity show the superconducting gap rapidly fills in. This also coincides with the 60 K plateau for a wide range of Ca- and La- substituted Y-123 samples and all of these features have been attributed to dynamic phase separation which freezes out at low temperature [31].

In the picture of electronic phase separation the underdoped cuprates evolve on doping into a phase with hole poor antiferromagnetic islands separated by grain boundaries of a hole rich "metallic" phase [32]. It is tempting to identify the antiferromagnetic island phase with domain size $L(p) \sim p^{-1/2}$ ($p^{-1/2}$ is the average distance between two holes) with the spin-glass phase. In this case the spin-glass transition temperature should be given by $T_g \sim J_{xy}(\xi_0/a)^2 \sim L^2 \sim 1/p$ in qualitative agreement with the experiment.

6. Conclusions

As an internal probe of the local fields in HTS cuprates the μ SR technique has proved to be a powerful tool for revealing many generic features in the magnetic phase behavior of these materials and the systematic changes in superfluid density with doping and substitution. Many of these were quite new results with important implications for the origins and physics of superconductivity while, for others, μ SR played a complementary role. In all cases the strength of the technique has been in investigating a systematic series of samples with progressive doping of one sort or another where spurious impurity phases and grain boundary effects do not affect the intrinsic response. The list is impressive: penetration depths, proximity-induced superconductivity, temperature- and scattering-dependent superfluid density, the symmetry of the order parameter, local moments and coexisting magnetism and superconductivity. It would be difficult to find another single technique for investigating HTS cuprates so broad in its compass and so rewarding in its use.

Acknowledgment

I am grateful to my many collaborators: C. Bernhard, T. Blasius, A. Golnik, A. Weidinger, J.I. Budnick, E.J. Ansaldo, J.L. Tallon, A. Moodenbaugh. The experiments described herein have been performed at the Paul Scherrer Institute, Villigen, Switzerland and TRIUMF, Vancouver. We thank these institutions and their support staff for continuing assistance. Funding assistance from the BMFB and the DFG is gratefully acknowledged.

References

- [1] For a review of the μ SR technique and application prior to HTSC see A. Schenck, *Muon Spin Rotation Spectroscopy*, Adam Hilger, Bristol 1985.
- [2] J.L. Tallon, C. Bernhard, H. Shaked, R.L. Hitterman, J.D. Jorgensen, *Phys. Rev. B* **51**, 12911 (1995).
- [3] W.K. Dawson, K. Tibbs, S.P. Weathersby, C. Boekema, K.-C.B. Chan, *J. Appl. Phys.* **64**, 5809 (1988).
- [4] W. Barford, J.M.F. Gunn, *Physica C* **156**, 515 (1988).
- [5] Y.J. Uemura, G.M. Luke, B.J. Sternlieb, J.H. Brewer, J.F. Carolan, W.N. Hardy, R. Kadono, J.R. Kempton, R.F. Kiefl, S.R. Kreitzman, P. Mulhern, T.M. Rise-man, D.Ll. Williams, B.X. Yang, S. Uchida, H. Takagi, J. Gopalakrishnan, A.W. Sleight, M.A. Subramanian, C.L. Chien, M.Z. Cieplak, Gang Xiao, V.Y. Lee, B.W. Statt, C.E. Stronach, W.J. Kossler, X.H. Yu, *Phys. Rev. Lett.* **62**, 2317 (1989).
- [6] Y.J. Uemura, L.P. Le, G.M. Luke, B.J. Sternlieb, W.D. Wu, J.H. Brewer, T.M. Rise-man, C.L. Seaman, M.B. Maple, M. Ishikawa, D.G. Hinks, J.D. Jorgensen, G. Saito, H. Yamochi, *Phys. Rev. Lett.* **66**, 2665 (1991).
- [7] J.W. Loram, K.A. Mirza, J.R. Cooper, W.Y. Liang, *Phys. Rev. Lett.* **71**, 1740 (1993).

- [8] V.J. Emery, S.A. Kivelsen, *Nature* **374**, 434 (1995).
- [9] Ch. Niedermayer, C. Bernhard, U. Binninger, H. Glückler, J.L. Tallon, E.J. Ansaldo, J.I. Budnick, *Phys. Rev. Lett.* **71**, 1764 (1993).
- [10] Ch. Niedermayer, C. Bernhard, U. Binninger, J.L. Tallon, E.J. Ansaldo, J.I. Budnick, *Phys. Rev. Lett.* **72**, 2502 (1994).
- [11] Y.J. Uemura, A. Keren, L.P. Le, G.M. Luke, W.D. Wu, Y. Kubo, T. Manako, Y. Shimakawa, M. Subramanian, J.L. Cobb, J.T. Markert, *Nature* **364**, 605 (1993).
- [12] C. Bernhard, Ch. Niedermayer, U. Binninger, A. Hofer, J.L. Tallon, G.V.M. Williams, E.J. Ansaldo, J.I. Budnick, *Physica C* **226**, 250 (1994).
- [13] J.M. Wade, J.W. Loram, K.A. Mirza, J.R. Cooper, J.L. Tallon, *J. Supercon.* **7**, 261 (1994).
- [14] C. Bernhard, Ch. Niedermayer, U. Binninger, A. Hofer, Ch. Wenger, J.L. Tallon, G.V.M. Williams, E.J. Ansaldo, J.I. Budnick, C.E. Stronach, D.R. Noakes, M.A. Blankson-Mills, *Phys. Rev. B* **52**, 10488 (1995).
- [15] M. Prenninger, R.G. Buckley, P. Keller, H.S. Barowski, A. Prueckl, M. Stumpf, E.V. Pechen, D.M. Pooke, K. Kishio, K.F. Renk, in: *Spectroscopic Studies of Superconductors*, Eds. I. Bozoric, D. van der Marel, SPIE, Bellingham 1996.
- [16] J.L. Tallon, C. Bernhard, U. Binninger, A. Hofer, G.V.M. Williams, E.J. Ansaldo, J.I. Budnick, Ch. Niedermayer, *Phys. Rev. Lett.* **74**, 1008 (1995).
- [17] D.N. Basov, R. Liang, D.A. Bonn, W.N. Hardy, B. Dabrowski, M. Quijada, D.B. Tanner, J.P. Rice, D.M. Ginsberg, T. Timusk, *Phys. Rev. Lett.* **74**, 598 (1995).
- [18] H. Lütgemeier, I. Heinmaa, D. Wagener, S.M. Hosseini, in: *Phase Separation in Cuprate Superconductors*, Eds. E. Sigmund, K.A. Müller, Springer, Berlin 1994, p. 225.
- [19] Y. Sun, K. Maki, *Phys. Rev. B* **51**, 6059 (1995).
- [20] K. Maki, in: *Superconductivity*, Ed. R.D. Parks, Vol. II, Marcel Dekker, New York 1969, p. 1035.
- [21] C. Bernhard, J.L. Tallon, C. Bucci, R. De Renzi, G. Guidi, G.V.M. Williams, Ch. Niedermayer, *Phys. Rev. Lett.* **77**, 2304 (1996).
- [22] J.I. Budnick, B. Chamberland, D.P. Yang, Ch. Niedermayer, A. Golnik, E. Recknagel, M. Rossmannith, A. Weidinger, *Europhys. Lett.* **5**, 65 (1988).
- [23] A. Weidinger, Ch. Niedermayer, A. Golnik, R. Simon, E. Recknagel, J.I. Budnick, B. Chamberland, C. Baines, *Phys. Rev. Lett.* **62**, 102 (1989).
- [24] N. Nishida, H. Miyatake, D. Shimada, S. Okuma, M. Ishikawa, T. Takabatake, Y. Nakazawa, Y. Kuno, R. Keitel, J.H. Brewer, T.M. Riseman, D.Ll. Williams, Y. Watanabe, T. Yamazaki, K. Nishiyama, K. Nagamine, E.J. Ansaldo, E. Torikai, *J. Phys. Soc. Jpn* **57**, 597 (1988).
- [25] A. Weidinger, Ch. Niedermayer, H. Glückler, A. Golnik, G. Nowitzke, E. Recknagel, H. Eickenbusch, W. Paulus, R. Schöllhorn, J.I. Budnick, *Hyperfine Interact.* **63**, 147 (1990).
- [26] F.C. Chou, F. Borsa, J.H. Cho, D.C. Johnston, A. Lascialfari, D.R. Torgeson, J. Ziolo, *Phys. Rev. Lett.* **71**, 2323 (1993).

- [27] F. Borsa, P. Carretta, J.H. Cho, F.C. Chou, Q. Hu, D.C. Johnston, A. Lascialfari, D.R. Torgeson, R.J. Gooding, N.M. Salem, K.J.E. Vos, *Phys. Rev. B* **52**, 7334 (1995).
- [28] R.J. Gooding, N.M. Salem, A. Mailhot, *Phys. Rev. B* **49**, 6067 (1994).
- [29] H. Casalta, H. Alloul, J.-F. Marucco, *Physica C* **204**, 331 (1993).
- [30] F.C. Chou, N.R. Belk, M.A. Kastner, R.J. Birgeneau, Amnon Aharony, *Phys. Rev. Lett.* **75**, 2204 (1995).
- [31] J.L. Tallon, N.E. Flower, G.V.M. Williams, to be published.
- [32] V.J. Emery, S.A. Kivelson, *Physica C* **209**, 597 (1993).